Research Square

Preprints are preliminary reports that have not undergone peer review.
They should not be considered conclusive, used to inform clinical practice,
or referenced by the media as validated information.

Aqueous organic anode//iodine cascadable battery with ultra-long lifespan, high energy and power density

Z.S. Zhang
South China Normal University
Yilong Zhu
The University of Adelaide
Miao Yu
Harbin Institute of Technology https://orcid.org/0000-0001-8820-9594
Yan Jiao
The University of Adelaide https://orcid.org/0000-0003-1329-4290
Yan Huang (yanhuanglib@hit.edu.cn)
Harbin Institute of Technology, Shenzhen https://orcid.org/0000-0003-4841-7262

Article

Keywords: Aqueous I2 battery, organic anode, cascade battery, ultra-long lifespan, high energy density, high power density

Posted Date: March 30th, 2022

DOI: https://doi.org/10.21203/rs.3.rs-1441754/v1

License: This work is licensed under a Creative Commons Attribution 4.0 International License.
Read Full License

Version of Record: A version of this preprint was published at Nature Communications on October 30th, 2022. See the published version at https://doi.org/10.1038/s41467-022-34303-8.

Abstract

Metal//iodine (I_2) batteries have sparked enormous interest as particularly promising energy storage devices. Still, the inherent dendrite growth and electrochemically inactive complexes formed with iodine anionic species at their metal anode make it challenging to substantially improve their performance. Herein, we report the first orgainc anode//I_2 battery. The battery delivers ultra-long lifespan (92000 cycles at 40 A g^{-1}), high rate tolerance (104 mAh g^{-1} at 160 A g^{-1}), energy density (434 Wh kg^{-1} at 50420 W kg^{-1}) and power density (155072 W kg^{-1} at 86 Wh kg^{-1}), far exceeding all the reported aqueous I_2-batteries. Moreover, the cascade form of this battery enables a voltage of 2.5 V without employing highly concentrated salts or polymer additives. This work addresses the major challenge of I_2-batteries and enriches the family of aqueous halogen-batteries with high performance and unlimited possibilities, and provides a new sight for the construction of high-performance battery systems based on sulfur electrodes.

Introduction

In recent years, rechargeable metal-halogen batteries, which rely on strict redox chemistry to achieve high energy and power density, have attracted considerable attention.[1–6] Superior to liquid bromine and gaseous chlorine, solid iodine (I_2) has better operability and stability.[7–10] Combining with its high abundance (50 – 60 μg/L_{ocean}), high theoretical capacity (422 mAh g^{-1}), high reversibility, and high theoretical redox potential of I^0/I^+ (1.07 V *vs.* standard hydrogen electrode), I_2 has stood out as a particularly promising cathode material for aqueous batteries.[3–6, 11–15] Moreover, the solid-liquid $I^-/I^0/I^+$ conversion of I_2 cathode avoids the issue of electrode collapse commonly occurred in intercalation counterparts.[5, 6, 14] Major success has been achieved on the development of various aqueous metal//I_2 batteries, *e.g.* Fe//I_2,[16] Al//I_2[17] and Zn//I_2.[3, 5, 6, 18–24] However, the intrinsic disadvantages of these batteries have also been recognized.[3–6, 12–21, 25] The inevitable dendrite growth and corrosion of the metal anodes cause rapid attenuation of capacity and short circuit; the leak-out iodine anionic species lead to formation of electrochemically inactive complexes with the metal anode, which induces the irreversibility of I_2 cathode and limited lifespan, similar to the shuttle effect in lithium-sulfur batteries.[3, 4, 26]

To address these issues, enormous efforts have been dovoted to modifying the metal anode and anchoring iodine species onto the cathode firmly,[5, 6, 12, 14, 16, 27, 28] leading to significant improvement. The best results obtained from the developed aqueous metal//I_2 batteries are 35000 cycles at 10.55 A g^{-1}, 23000 cycles at 6 A g^{-1}, 6000 cycles at 1.92 A g^{-1} for cycling,[6, 18, 21] 109100 W kg^{-1} at 179 Wh kg^{-1} and 410 Wh kg^{-1} at 110 W kg^{-1} for Ragone performance,[20, 21] and 140 mAh g^{-1} at 21 A g^{-1} and 419 mAh g^{-1} at 2 A g^{-1} for rate performance.[3, 21] However, it remains highly challenging to substantially boost the performance of metal//I_2 batteries. A novel alternative system has been proposed recently, *i.e.* replacing

the anode materials to be hydrogen (H_2).[14] The H_2//I_2 system delivers new promise but showing certain limits: it requires a swagelok cell involving complicated fabrication and expensive Pt/C catalysts; meanwhile, the cell voltage is < 1.2 V, and the capacity is ~ 0.5 mAh at 2.5 mA cm^{-2}. A breakthrough strategy is, therefore, pressingly needed to significantly improve the lifespan, energy density and power density of I_2-cathode batteries.

Integrating two or more batteries together is the common route to attain higher capacity and energy density. In fact, when the batteries are integrated through external wires, their performance is often compromised. In this regard, the cascade battery, integrating two or more battery reactions inside a single battery, holds obvious advantages, as it avoids the non-electrochemically active connection required for external integration and can effectively increase the energy output. Lately, Dai *et al.* has proposed the first successful precedent of a cascade battery based on Zn//S system.[29] Still, the feasbility of extending the cascade form to other battery systems remains unexplored.

Herein, we report the first organic anode//I_2 battery and its cascade system. Distinct from the reported aqueous metal//I_2 and H_2//I_2 battery systems, 3,4,9,10 – Perylenetetracarboxylic diimide (PTCDI) is employed as the anode material. Thanks to the intrinsic inertness of the PTCDI anode to various iodine anionic species and the fast conversion of $I^-/I^0/I^+$ in the saturated potassium chloride (KCl) electrolyte, ultra-long lifespan (92000 cycles at 40 A g^{-1}) and remarkably high rate tolerance (104 mAh g^{-1} at 160 A g^{-1}), high energy density (434 Wh kg^{-1} at 50420 W kg^{-1}) and high power density (155072 W kg^{-1} at 86 Wh kg^{-1}) have been achieved simultaneously, far exceeding those of the aqueous I_2-cathode batteries ever reported and most reported aqueous K^+ ions batteries. Moreover, by evolving into the cascade form with saturated mixture of KCl + I_2(aq) as electrolyte, the voltage further reaches 2.5 V without employing highly concentrated salts or polymer additives. By replacing metal anode with organic compound and constructing the the cascade system, this work opens up a fertile ground for high-performance aqueous I_2-cathode batteries, and promotes the application potential of halogen batteries towards industry and market. Besides, this work also provides a new sight for the construction of high-performance battery systems based on sulfur electrodes.

Results And Discussion

The key to construct the novel high-performance I_2-cathode battery lies in two aspects: electrolyte and anode. Concerning the selection of aqueous electrolyte, it should guarantee the highest conversion efficiency of $I^-/I^0/I^+$, so that give full play to the potential advantages of high theoretical capacity and redox potential of the I_2 cathode. That is to say, for the I^-/I^0 conversion, the cation in the electrolyte must reduce the conversion energy barrier. As a result, the discharge voltage could be promoted due to the reduced polarization.[5] For the I^0/I^+ conversion, the anion in the selected electrolyte must benefit the dissociation of I^+ compounds so as to accelerate the I^0/I^+ conversion.[2, 3, 5] Regarding the anode, only when it satisfies simultaneously the demands of high structural stability, immunity to various iodine

anionic species, low redox potential, high capacity and low cost, all issues of the two reported I_2-cathode battery systems mentioned above can be ultimately avoided. Compared with inorganic materials, organic materials featuring structural diversity, flexible molecular stucture and low cost are a promising candidate for this novel aqueous I_2-cathode battery system.[30–33]

Density Functional Theory (DFT) calculations were performed to predict reaction energy profiles of I^-/I^0 conversion with the existence of different cations within the electrolyte, for the selection of cation candidate. In addition, the dissociation energy of I_nX (X denotes anion of electrolyte, n denotes electron number) were compared in different anions environment, to identify the best anion. As shown in Fig. 1a, the lowest value of Gibbs free energy change (ΔG) is observed when the I^-/I^0 conversion chemistry occurs in K^+ environment. Thus, the aqueous electrolyte containing K^+ should hold great potential due to the fastest reaction rate of the I^-/I^0 conversion.[5, 20] For anions, the lowest dissociation energy of ICl is evidently observed when compared to that of other iodides, indicating the fast conversion of I^0/I^+ in aqueous electrolyte containing Cl^- (Fig. 1b).[2, 3, 5] Accordingly, the aqueous KCl electrolyte should well guarantee high performances of I_2 cathode. Moreover, linear sweep voltammetry (LSV) test shows that the total operational voltage window is up to 2.72 V in saturated KCl electrolyte, which is large enough to match most aqueous batteries (Fig. S1). [12, 34–36]

Then, it is necessary to determine an appropriate anode that can insert/release K^+ reversibly in aqueous electrolyte. Due to the sluggish kinetics of the larger Cl^- compared with K^+, materials capable of intercalation/de-intercalation of Cl^- were ruled out.[37] As shown in Fig. 1c, organic aromatic molecules with diverse number of aromatic rings and carbonyl groups (DPPZ,[38] β-PTCDA,[38] PNTCDA,[39] PT[32]), inorganic and composite materials ($KTi_2(PO_4)_3$,[40] KPB@PPy[41]) were compared. Clearly, PTCDI (3,4,9,10-Perylenetetracarboxylic diimide) displays the lowest redox potential and highest specific capacity, thus holding a great promise as anode in the aqueous KCl electrolyte.[34, 42] X – ray diffraction (XRD) and Fourier transform infrared (FT-IR) spectroscopy were performed to determine the crystal structure and functional groups of PTCDI (Fig. S2). Besides, electrochemical performances of PTCDI electrode were investigated in saturated KCl electrolyte (Fig. S3 – 4). These results confirmed the highly reversible insertion/extraction of K^+ owing to the large interplanar distance of PTCDI (Fig. S5).[34, 43, 44]

Based on materials screened above, the aqueous PTCDI//I_2 full cell was assembled with PTCDI as anode, I_2 facilely sublimated on active carbon (AC) as cathode (I_2@AC, Fig. S6) and saturated KCl solution as electrolyte. Considering the theoretical capacity of I_2 (422 mAh g^{-1}) [3, 9, 28] and PTCDI (137 mAh g^{-1})[43], a mass ratio of PTCDI:I_2 = 3.1 is utilized. The PTCDI//I_2 full cell displays a significant advantage in making full use of anode when compared with the conventional metal//I_2 battery system. During the charge/discharge process, the oxidation/reduction reaction of $I^-/I^0/I^+$ occurs at the I_2@AC cathode and the enolization/recovery of carbonyl groups occurs at the PTCDI anode with K^+ intercalation/de-

intercalation (Fig. 2a-b).[2, 3, 5] Hence, the chemical equations of the PTCDI//I_2 full cell in saturated KCl can be described as below:

Cathode: $2I^- \leftrightarrow I_2 + 2e^-$ $I_2 + 2Cl^- \leftrightarrow 2ICl + 2e^-$ (1)

Anode: $2PTCDI + 4K^+ + 4e^- \leftrightarrow 2PTCDI - 2K$ (2)

With the increase of cycle numbers, the initial redox peaks shifted toward positive direction gradually and finally stabilized due to the activation process (Fig. S7a).[26, 45, 46] Consequently, typical CV curves of PTCDI//I_2 within the voltage range of 0 – 2.4 V are presented (Fig. 2c, Fig. S7b-d). Oxidation peaks at 1.54 V, 2.24 V and reduction peaks of 1.71 V, 0.91 V, 0.72 V are clearly observed. As for the I_2@AC cathode, the redox pair of 2.24 V/1.71 V corresponds to the reversible reaction of I^0/I^+ while the rest redox pairs correspond to the reversible transformation between I^- and I^0. [2, 3, 5] As for the PTCDI anode, the anodic and cathodic peaks correspond to the stepwise intercalation and de-intercalation of K^+.[34, 42, 44] The typical galvanostatic charge/discharge (GCD) curve displays a major plateau at 1.90 V during the discharge process (Fig. 2d). Impressively, the voltage plateau of the PTCDI//I_2 full cell is of considerable superiority to that of all reported aqueous rechargeable Zn//I_2,[3, 5, 6, 18–21, 47] Fe//I_2[16], Al//I_2,[17] H_2//I_2,[48] and most aqueous rechargeable K^+ full battery systems (ARKFBs),[38–42] making it a promising prospect for high-energy output (Fig. 2e).

As shown in Fig. 2f, the cycling performance of the PTCDI//I_2 full cell was further investigated by GCD mode at 40 A g^{-1} and the specific capacity was calculated based on the mass of I_2 in I_2@AC cathode. Notably, discharge capacity of 364 mAh g^{-1} was delivered after initial activation process. Such a high discharge capacity originates from the full use of $I^-/I^0/I^+$ conversion reactions.[2, 3, 5] Remarkably, 154 mAh g^{-1} of discharge capacity was obtained after 92000 cycles at 40 A g^{-1} (Fig. 2f), far exceeding all reported I_2-based aqueous batteries[3, 5, 6, 16–21, 47, 49–54] and most ARKFBs[38, 40–42] whatever the aspect of the comparison (Fig. 2g). Such an ultra-long lifespan with high capacity at high rate is attributed to the nature of inertness to iodine anions and the layered structure of the PTCDI anode with large interplanar spacing. Apart from that, the highly reversible enolization of quinone (– C = O) to quinone salts (– C–O – M) is propitious to maintain the structural stability of the PTCDI anode during repeated cycles and thus favors the cycling performance of the full cell.[34] To figure out the capacity contribution of AC, GCD of the PTCDI//AC full cell was tested and only 38 mAh g^{-1} of discharge capacity was delivered, verifying the fact that capacity contribution of AC is not significant at all (Fig. S8).[3]

As illustrated in Fig. 2h, the rate capability of PTCDI//I_2 full cell was investigated under varied current densities from 40 A g^{-1} to 160 A g^{-1}. In detail, discharge capacities of 323, 204, 140, 116 and 104 mAh g^{-1} were delivered at 40, 70, 100, 130 and 160 A g^{-1}, respectively. Remarkably, a discharge capacity of 322 mAh g^{-1} was achieved when the current density was shifted from 160 A g^{-1} to 40 A g^{-1}, which is 99.7% of the initial specific capacity, validating the outstanding rate capability of the full cell and in

accord with the CV results in Fig. S7. As shown in Fig. 2i, the demonstrated rate capability of the full cell surpasses all reported I_2-based cathode batteries[3, 5, 6, 16–21, 47, 49–54] and ARKFBs[38, 40–42], representing the highest level thus far. As presented in Fig. 2j, the full cell can exhibit an energy density of 434 Wh kg^{-1} at a power density of 50420 W kg^{-1}. Moreover, an energy density of 86 Wh kg^{-1} can be maintained when operated at the peak power density of 155072 W kg^{-1}. Furthermore, the energy density and power density of the full cell far exceed those of all reported aqueous batteries with I_2-based cathode[6, 14, 16, 20, 21, 27, 28, 55, 56] and most ARKFBs[38, 57], possessing a very promising prospect in practical application. Accordingly, the record ultra-long lifespan, remarkable Ragone performances and high rate tolerance of the PTCDI//I_2 full cell successfully demonstrate the superiority of the intrinsic inertness of the PTCDI anode to various iodine anionic species and the fast conversion of $I^-/I^0/I^+$ in the saturated KCl electrolyte, addressing the major challenge of the reported aqueous I_2-batteries. The results achieved promote the electrochemical performance of aqueous I_2-batteries to a new epoch. Moreover, considering the multi-variety and multi-function of organic materials, the first introduction of PTCDI organic anode into aqueous I_2-batteries not only enriches the family of aqueous halogen-batteries with high performance, but also brings about enormous markets for the use of halogen electrode in the near future. Furthermore, the strategy of selecting PTCDI organic material as anode provides a new sight for the construction of high-performance battery systems based on sulfur electrodes.

To identify the underlying redox chemistry of the two-electron transfer of the I_2 cathode, ultraviolet-visible (UV-vis) and Raman spectroscopy were performed. Figure 3a displays the typical GCD curve of the PTCDI//I_2 full cell at 40 A g^{-1} marked with selected voltage points for characterizations. As illustrated in Fig. 3b, a broad absorption peak in the range from 375 nm to 494 nm corresponding to the formation of iodine molecules when charged to 2.0 V, confirming the conversion from iodide to iodine. It is noted that no characteristic peak of I_3^- (290 nm) was observed, indicating a direct conversion between I^- and I^0.[2, 3, 5] A new strong peak (341 nm) corresponding to the formation of ICl interhalogens was clearly observed when charged to 2.4 V, verifying the conversion of I^0 to I^+. Meanwhile, the adsorption peak of iodine molecule (375 – 494 nm) vanished when charged to 2.4 V, consolidating the oxidation process from I^0 to I^+. Correspondingly, the characteristic adsorption peaks almost recovered to the original state during the discharge process, verifying the highly reversible conversion of $I^-/I^0/I^+$.[2, 3, 5] As shown in Fig. 3c, a new Raman signal (208 cm^{-1}) corresponding to the characteristic band of ICl interhalogens emerged when charged to 2.4 V, and vanished when discharged to 1.25 V, consolidating the reversible I^0/I^+ conversion and in accord with UV-vis results in Fig. 3b. [2, 3, 5, 58]

To better study the energy storage mechanism of the PTCDI anode, X-ray photoelectron spectroscopy (XPS) and FT-IR were performed at different states. As illustrated in Fig. 3d, the strong characteristic peaks of K 2*p* emerged at the fully charged state while no signal peaks were detected at pristine state, demonstrating the successful intercalation of K^+ into PTCDI. Conversely, the intensity of K 2*p* peaks at the fully discharged state declined sharply and almost vanished when compared with that at the fully

charged state, verifying the reversible de-intercalation of K^+ from PTCDI.[31, 34, 42, 44] Distinct from the pristine state, a new peak (532.6 eV) corresponding to the C – O species at the fully charged state was clearly observed, verifying the conversion of C = O to C – O species (Fig. 3e).[31, 32, 34, 39, 42–44, 59] During the subsequent discharge process, the relative intensity of C – O/C = O declined from 1.32 at the fully charged state to 0.12, demonstrating the reversible conversion of C – O to C = O species. Apart from that, the reversible conversion process of the PTCDI anode was also consolidated by FT-IR (Fig. 3f). It is notable that the intensity of the stretching vibration of carbonyl groups (– C = O) appearing at 1666 cm^{-1} at the fully charged state is significantly weaker than that at pristine state. Meanwhile, a new and broad peak standing at 1617 cm^{-1} can be clearly observed, demonstrating the conversion from carbonyl groups (– C = O) to enolate groups (– C–O).[31, 32, 34, 39, 42–44, 59] Upon the subsequent discharge process, almost all the above characteristic peaks recovered to their original positions and intensities, suggesting the highly reversible conversion between carbonyl (– C = O) and enolate (– C–O) groups of the PTCDI anode.

Considering the intrinsic superiority of being inert to various iodine anionic species of the PTCDI anode and superb electrochemical performances of the PTCDI//I_2 full cell in saturated KCl electrolyte, an additional saturated I_2(s) was introduced into the KCl electrolyte to validate the feasibility of the PTCDI//I_2 full cell in the presence of I_2 in electrolyte. Herein, distinct from various strategies employed in metal//I_2 batteries that try best to confine I_2 in cathode to prevent iodine species from entering the electrolyte, whichever in fact cannot completely prevent, the PTCDI//I_2 full cell has no need to worry about this knotty problem and even welcome the introduction of I_2 into electrolyte. The operational voltage window of the saturated KCl + I_2(aq) mixed electrolyte was 2.75 V, slightly broader than that of pure saturated KCl electrolyte which may ascribe to the less amount of free water when saturated I_2 is dissolved in the electrolyte (Fig. S9).[60] As expected, CV curves of the PTCDI electrode in the mixed electrolyte were identical to that in pure saturated KCl electrolyte, consolidating the intrinsic characteristics of inertness to various iodine anionic species of the PTCDI electrode (Fig. S10a). As a control experiment, CV measurement of the PTCDI electrode was also performed in a pH ≈ 5 dilute HCl electrolyte (the same pH value as the mixed electrolyte) and no redox peaks are observed, indicating that protons have no effect on the charge/discharge of the PTCDI electrode (Fig. S10b).

Figure 4a displays typical CV curve of the PTCDI//I_2 full cell in the saturated KCl + I_2(aq) mixed electrolyte. Strikingly, a cascade cell composed of two independent electrochemical processes (marked as step 1 and step 2 separately) is clearly observed. Compared with conventional batteries including only one electrochemical reaction, this cascade battery presents many advantages: *a*, integrating two full reactions internally and avoiding the inactive additional components needed for external connection. *b*, higher utilization of the reaction chamber. *c*, higher energy output.[29] The CV curve in step 2 is in consistent with that of the PTCDI//I_2 full cell in pure saturated KCl electrolyte. Apart from that, a pair of additional redox peaks in step 1 is attributed to the I_2//I_2 symmetric cell self-constructed in the mixed electrolyte and is discussed as follows. When using a blank graphite paper (GP, current collector in the above-discussed PTCDI//I_2 batteries) as working electrode tested in the mixed electrolyte, two pairs of redox peaks

corresponding to the conversion of I^-/I^0 and I^0/I^+ are apparent, which means the existence of the possibility of $I_2//I_2$ symmetric cell self-constructed in the mixed electrolyte (Fig. S11).[2, 3, 5] Then, two pairs of redox peaks centered at different potentials are clearly separated (Fig. 4b). Therefore, a pair of pronounced redox peaks within the voltage range of 0 – 0.5 V is clearly detected when using blank GP as both electrodes in the full cell, demonstrating that the $I_2//I_2$ symmetric cell self-constructs successfully in the mixed electrolyte (Fig. 4c). Moreover, the voltage range of the $I_2//I_2$ symmetric cell is consistent with that of step 1 in Fig. 4a, further confirming that the redox peaks in step 1 are assigned to the $I_2//I_2$ symmetric cell. Besides, no characteristic redox peaks of the blank GP//GP full cell were detected whether in pure saturated KCl electrolyte (Fig. S12a) or in pure saturated I_2(aq) electrolyte (Fig. S12b), verifying that the $I_2//I_2$ symmetric cell self-constructed only in the mixed electrolyte. Fig. S12b also substantiates the importance of Cl^- in electrolyte and in accord with the theoretical calculation results in Fig. 1b.

As an indispensable part of the PTCDI//I_2 cascade cell system, electrochemical performances of the $I_2//I_2$ symmetric cell (step 1) were systematically evaluated by testing the GP//GP full cell in the mixed electrolyte (Fig. S13). During the charge process, I_2 molecules absorbed at the interface between the anode and electrolyte were oxidized to I^+ while absorbed at the interface between the cathode and electrolyte were reduced to I^- simultaneously (Fig. S13a).[2, 3, 5] Reversibly, all the above oxidized and reduced states of iodine recovered to their original state individually during the discharge process (Fig. S13b). A charge plateau at 0.38 V and a discharge plateau at 0.19 V were clearly observed in the typical GCD curve of the $I_2//I_2$ symmetric cell (Fig. S13c), in accord with the CV results in Fig. 4c. A discharge areal capacity of 0.06 mAh cm^{-2} can be obtained at 0.2 mA cm^{-2} after 9930 cycles, exhibiting the excellent stability of the $I_2//I_2$ symmetric cell. Distinct from conventional batteries, the capacity exhibits a trend of continuous rise during cycling due to the increasing activated I_2 molecules (Fig. S13d). Moreover, discharge areal capacities of 0.03, 0.016, 0.008 and 0.006 mAh cm^{-2} were achieved at 2, 5, 10 and 15 mA cm^{-2}, respectively, indicating good rate capability (Fig. S13e). A new peak centered at 343 nm corresponding to ICl interhalogens emerged at the fully charged state and almost vanished at the fully discharged state, verifying the reversible conversion of I^0/I^+ (Fig. S13f).[2, 3, 5] In view of a large amount of I_2 contained in the mixed electrolyte, the intensity change of the broad absorption peak (375 – 494 nm) corresponding to I_2 molecules was not apparent at different states.[2, 3, 5]

Therefore, the first charge step (marked as step 1) of the cascade cell based on the PTCDI//I_2 in the saturated KCl + I_2(aq) mixed electrolyte corresponds to the conversion of the $I_2//I_2$ symmetric cell within the voltage range of 0 – 0.5 V (Fig. 4e). During the second charge step (marked as step 2) within the voltage range of 0.5 – 2.5 V, the conversion of $I^-/I^0/I^+$ occurred at the cathode and the intercalation of K^+ occurred at the PTCDI anode (Fig. 4f).[2, 3, 5] Overall, chemical reactions of the cascade cell can be expressed as follows:

Step 1: cathode: $I_2 + 2Cl^- \leftrightarrow 2ICl + 2e^-$ (3)

anode: $I_2 + 2e^- \leftrightarrow 2I^-$ (4)

Step 2: cathode: $2I^- \leftrightarrow I_2 + 2e^-$ $I_2 + 2Cl^- \leftrightarrow 2ICl + 2e^-$ (5)

anode: $2PTCDI + 4K^+ + 4e^- \leftrightarrow 2PTCDI - 2K$ (6)

As presented in Fig. 4g, a major discharge plateau at 0.34 V corresponding to the $I_2//I_2$ symmetric cell was clearly observed in step 1, and the GCD curve in step 2 was identical to that of the PTCDI//I_2 full cell in saturated KCl electrolyte in Fig. 2d. Moreover, these results are in accord with CV results in Fig. 4a, and consolidate the successful construction of the PTCDI//I_2 cascade cell in the mixed electrolyte. A high discharge capacity of 623 mAh g^{-1} was delivered at 40 A g^{-1} after 6000 cycles (Fig. 4h). Impressively, the PTCDI//I_2 cascade cell even achieved 105000 cycles under a higher current density of 60 A g^{-1}, exhibiting an outstanding cyclical stability (Fig. S14). The morphology and particle size of the PTCDI anode after cycling at 40 A g^{-1} for 9200 cycles in the mixed electrolyte are almost identical to those in pristine state, consolidating the intrinsic superiority of being immune to various iodine anionic species and excellent structural stability of PTCDI (Fig. S15). As illustrated in Fig. 4i, discharge capacities of 574, 500, 376, 285 and 264 mAh g^{-1} were delivered at 40, 70, 100, 130 and 160 A g^{-1}, respectively. Notably, a discharge capacity of 572 mAh g^{-1} was delivered when the current density was shifted from 160 to 40 A g^{-1}, the value of which is 99.7% of that at initial 40 A g^{-1}, demonstrating the superb rate capability of the PTCDI//I_2 cascade cell. Compared with well-known strategies (e.g., water-in-salt, liquid polymer additive)[61–80] to broaden the voltage window in aqueous electrolyte, the high voltage of the PTCDI//I_2 cascade cell exhibited great superiority by just utilizing the saturated KCl + I_2(aq) mixed electrolyte without highly concentrated salts or a large amount of polymers (Fig. 4j). Consequently, this is a promising strategy to obtain a low-cost, eco-friendly and high-voltage aqueous battery. Therefore, distinct from the reported I_2-cathode single battery, the successful construction of PTCDI//I_2 cascade cell in mixed electrolyte for the first time demonstrates the feasibility of cascade cell in I_2-batteries, making full use of the iodine leaked from the I_2 cathode and outputting more energy as $I_2//I_2$ symmetric cell in electrolyte. Moreover, the concept of PTCDI//I_2 cascade cell not only enriches the family of aqueous halogen-batteries with high performance, but also paves a new way for the construction of high-performance battery systems based on sulfur electrodes.

Inspired by the results that the conversion of $I^-/I^0/I^+$ can be completed by merely using blank GP as electrode in the mixed electrolyte (Fig. S11), an aqueous cathode-free cascade cell of PTCDI//GP was successfully constructed in the same electrolyte (Fig. S16). Owing to the same reaction mechanism, reaction processes of the PTCDI//GP cathode-free cascade cell are identical to those of the PTCDI//I_2 cascade cell (Fig. S16a – f). Similarly, the PTCDI//GP cathode-free cascade cell demonstrated stable cycling performance and good rate capability (Fig. S16g – i). Furthermore, a large area soft package battery of the PTCDI//GP cathode-free cascade cell with 6 cm · 8 cm was successfully assembled (Fig. 4k). The capacity retention reached 70% at 80 mA after cycling for 900 cycles, exhibiting good

cyclical stability (Fig. 4l). A power density of 52 W m^{-2} was obtained when an ultra-high current of 320 mA was applied, indicating the high rate tolerance of the cascade cell. Besides, a power density of 16 W m^{-2} was achieved when the current was shifted from 320 to 80 mA, the value of which is almost identical to that at initial 80 mA, exhibiting good reversibility (Fig. 4m).

Conclusion

In summary, unlike all the reported aqueous I_2-cathode batteries, a novel aqueous PTCDI//I_2 battery in saturated KCl electrolyte was firstly proposed. Strikingly, owing to the intrinsic superiority of inertness to various iodine anionic species and excellent structural stability of the PTCDI anode as well as the efficient conversion of $I^-/I^0/I^+$ benefiting from the KCl electrolyte, an ultra-long lifespan up to 92000 cycles of the full cell under the high current density of 40 A g^{-1} was achieved. Besides, the maximal energy density and power density can be reached to 434 Wh kg^{-1} at 50420 W kg^{-1} and 155072 W kg^{-1} at 86 Wh kg^{-1}, respectively, far exceeding all reported I_2 – based cathode batteries and most ARKFBs. Furthermore, considering the characteristics of intrinsic inertness to various iodine anionic species of PTCDI, the PTCDI//I_2 battery welcomed the introduction of I_2 into electrolyte and successfully self-constructed a cascade cell in KCl + I_2(aq) mixed electrolyte, which can further reach 2.5 V without employing highly concentrated salts or polymer additives and work for 105000 cycles at 60 A g^{-1}, providing new sights for constructing two-in-one battery systems. Moreover, in view of the results that the conversion of $I^-/I^0/I^+$ can be completed when just using blank GP current collector as electrode in the mixed electrolyte, the PTCDI//GP cathode-free cascade cell was firstly constructed. Besides, a soft package battery with large area of the PTCDI//GP cathode-free cascade cell was evaluated. The design of this novel ultra-high-performance PTCDI//I_2 full cell and its cascade system broadens the family of aqueous I_2-cathode battery systems, lays a solid foundation towards industry and market, and provides a new idea for the construction of high-performance battery systems based on halogen and sulfur electrodes.

Methods

Chemicals and materials synthesis. Iodine (I_2; ≥ 99.8%, Aladdin, China), potassium chloride (KCl; 99%, Aladdin, China), 3,4,9,10 – Perylenetetracarboxylic diimide (PTCDI; 95%, Alfa Aesar, America), active carbon (AC; 1800 m^2 g^{-1}, XFNANO, China) were purchased and used without further treatment. I_2@AC was synthesized through a facile method. Briefly, equal amount of I_2 and AC were entirely mixed by grinding. Then, the mixed powder was sealed in a hydrothermal reactor and heated at 80 ℃ for 4 h. After natural cooling, porous I_2@AC was obtained.

Preparation of electrodes. To prepare the PTCDI anode, PTCDI, Ketjen Black (KB) and polyvinylidene fluoride (PVDF) binder were homogeneously mixed at a weight ratio of 7:2:1 in N – methyl pyrrolidone (NMP) solvent. After stirring for 4 h, the mixture was coated onto a graphite paper (GP) substrate and

dried under vacuum at 80 ℃ for 12 h. The average mass loading of the PTCDI anode is 1.0 – 1.3 mg cm^{-2}.

To prepare the I_2@AC cathode, I_2@AC, KB and PVDF binder were homogeneously mixed at a weight ratio of 8:1:1 in NMP solvent. After stirring for 4 h, the mixture was coated onto a GP substrate and dried under vacuum at 40 ℃ for 12 h. The average mass loading of the I_2@AC cathode is 0.5 – 0.7 mg cm^{-2}.

To prepare the AC electrode, AC, KB and PVDF binder were homogeneously mixed at a weight ratio of 7:2:1 in NMP solvent. After stirring for 4 h, the mixture was coated onto a GP substrate and dried under vacuum at 80 ℃ for 12 h. The average mass loading of the AC electrode is 1.0 – 1.3 mg cm^{-2}.

To prepare the KB electrode, KB and PVDF binder were homogeneously mixed at a weight ratio of 9:1 in NMP solvent. After stirring for 4 h, the mixture was coated onto a GP substrate and dried under vacuum at 80 ℃ for 12 h. The average mass loading of the KB electrode is 1.0 – 1.3 mg cm^{-2}.

Materials charaterization and electrochemical measurements. X – ray diffraction (XRD; Ultima IV, Rigaku, Japan) was carried out to determine the structure and phase composition. Fourier transform infrared spectroscopy (FT – IR; Nicolet iS5, Thermo Scientific, America) was performed to determine the functional groups of organic molecule. Brunaur – Emmett – Teller (BET; ASAP 2460, Quantachrome, America) surface areas were measured using N_2 adsorption – desorption at 77 K. Ultraviolet – visible (UV – vis; Lambda 365, Perkin Elmer, America) spectroscopy was carried out with a range from 200 to 800 nm. Raman spectroscopy (Qontor, Renishaw/InVia, England) equipped with a laser of 532 nm wavelength was conducted to record the crystallographic information. X – ray photoelectron spectroscopy (XPS; PHI 5000 Versaprobe III, Ulvac – Phi, Japan) was performed to analyze the surface composition and valance evolution details. Scanning electron scanning electron microscopy (SEM; SU8010, HITACHI, Japan) was employed to characterize the morphology. Cyclic voltammetry (CV) and linear sweep voltammetry (LSV) test were carried out on a electrochemical workstation (CHI760E, Chenhua, China). The electrochemical potential window of the aqueous electrolyte was determined through the three-electrode system (working electrode: the KB electrode; counter electrode: platinum; reference electrode: standard Ag/AgCl electrode). Galvanostatic charge/discharge (GCD) measurement was conducted in a battery test system (CT3002A, LANHE, China).

Computational details. All structures were optimized by Density Functional Theory (DFT) using B3LYP functional with LANL2DZ basis set, using Gaussian 09W program.[81, 82] All calculations were carried out with the atom-pairwise dispersion correction (DFT-D3) and the implicit universal solvation model based on Solute Electron Density (SMD).[83, 84]

To clarify the mechanism of selected cations on the conversion of I^-/I^0, several systems were simulated, and the Gibbs free energy change (ΔG) was used to measure the degree of spontaneity of different systems (formula shows below).

$$\Delta G = \mathrm{G}_{product} - \mathrm{G}_{reactant}$$

The dissociation energy ($E_{dissociation}$) were computed from:

$$\mathrm{E}_{dissociation} = \mathrm{E}_{anion} + \mathrm{E}_{I} - E_{group}$$

E_{group}, E_I and E_{anion} are the energies of the group, I^+ ion and isolated anions, respectively.

Data Avaliability

The data that support the plots within these paper and other findings of this study are available from the corresponding author on reasonable request. Source data are provided with this paper.

Declarations

Acknowledgements

This research was supported by the Natural Science Foundation of Guangdong Province for Distinguished Young Scholars (No. 2018B030306022), the Project of International Science and Technology Cooperation in Guangdong Province (No. 2020A0505100016), the Shenzhen Sauvage Nobel Laureate Laboratory for Smart Materials, and Shenzhen Science and Technology Program (No. KQTD20200820113045083).

Author contributions

Y. H., M.Y. and Z.S.Z. designed the research. Z.S.Z. conducted material preparations, electrochemical tests and characterizations. Y.L.Z. and Y.J. conducted the computations. Z.S.Z., Y. H., M.Y. and Y.J. prepared the manuscript. All authors contributed to the discussion of the data.

Competing interests

The authors declare no competing interests.

References

1. Li, P. et al. Highly Thermally/Electrochemically Stable I^-/I_3^- Bonded Organic Salts with High I Content for Long-Life Li-I_2 Batteries. Adv. Energy Mater. (2022).
2. Li, X. et al. Two-Electron Redox Chemistry Enabled High-Performance Iodide-Ion Conversion Battery. Angew. Chem. Int. Ed. (2022).
3. Zou, Y. et al. A four-electron Zn-I_2 aqueous battery enabled by reversible $I^-/I_2/I^+$ conversion. Nat. Commun. **12** (2021).

4. Ma, J., Liu, M., He, Y. & Zhang, J. Iodine Redox Chemistry in Rechargeable Batteries. Angew. Chem. Int. Ed. **60**, 12636–12647 (2021).
5. Li, X. et al. Activating the I^0/I^+ redox couple in an aqueous I_2-Zn battery to achieve a high voltage plateau. Energy Environ. Sci. **14**, 407–413 (2021).
6. Li, X. et al. Enhanced Redox Kinetics and Duration of Aqueous I_2/I^- Conversion Chemistry by MXene Confinement. Adv. Mater. **33** (2021).
7. Li, X. et al. A Complexing Agent to Enable a Wide-Temperature Range Bromine-Based Flow Battery for Stationary Energy Storage. Adv. Funct. Mater. **31** (2021).
8. Lu, W. et al. Multifunctional Carbon Felt Electrode with N-Rich Defects Enables a Long-Cycle Zinc-Bromine Flow Battery with Ultrahigh Power Density. Adv. Funct. Mater. **31** (2021).
9. Lee, J.-H. et al. High-Energy Efficiency Membraneless Flowless Zn-Br Battery: Utilizing the Electrochemical-Chemical Growth of Polybromides. Adv. Mater. **31** (2019).
10. Li, X. et al. Confining Aqueous Zn-Br Halide Redox Chemistry by $Ti_3C_2T_x$ MXene. ACS Nano **15**, 1718–1726 (2021).
11. Jeon, J., Hwang, J., Yang, J.H. & Chang, J. Electrochemical formation and dissolution of an iodine-halide coordination solid complex in a nano-confined space. J. Mater. Chem. A **9**, 17955–17966 (2021).
12. Shang, W. et al. Establishing High-Performance Quasi-Solid Zn/I_2 Batteries with Alginate-Based Hydrogel Electrolytes. ACS Appl. Mater. Interfaces **13**, 24756–24764 (2021).
13. Zhao, Q., Lu, Y., Zhu, Z., Tao, Z. & Chen, J. Rechargeable Lithium-Iodine Batteries with Iodine/Nanoporous Carbon Cathode. Nano Lett. **15**, 5982–5987 (2015).
14. Pan, H. et al. Controlling Solid-Liquid Conversion Reactions for a Highly Reversible Aqueous Zinc-Iodine Battery. ACS Energy Lett. **2**, 2674–2680 (2017).
15. Zhang, F., Wang, Q. & Tang, Y. Extended iodine chemistry: Toward high-energy-density aqueous zinc-ion batteries. Matter **4**, 2637–2639 (2021).
16. Bai, C., Jin, H., Gong, Z., Liu, X. & Yuan, Z. A high-power aqueous rechargeable Fe-I_2 battery. Energy Stor. Mater. **28**, 247–254 (2020).
17. Yang, S. et al. High-Rate Aqueous Aluminum-ton Batteries Enabled by Confined Iodine Conversion Chemistry. Small Methods **5** (2021).
18. Yang, H. et al. A Metal-Organic Framework as a Multifunctional Ionic Sieve Membrane for Long-Life Aqueous Zinc-Iodide Batteries. Adv. Mater. **32** (2020).
19. Yu, D., Kumar, A., Tuan Anh, N., Nazir, M.T. & Yasin, G. High-Voltage and Ultrastable Aqueous Zinc-Iodine Battery Enabled by N-Doped Carbon Materials: Revealing the Contributions of Nitrogen Configurations. ACS Sustain. Chem. Eng. **8**, 13769–13776 (2020).
20. Ma, L. et al. Electrocatalytic Iodine Reduction Reaction Enabled by Aqueous Zinc-Iodine Battery with Improved Power and Energy Densities. Angew. Chem. Int. Ed. **60**, 3791–3798 (2021).

21. Chen, C. et al. High-Energy Density Aqueous Zinc-Iodine Batteries with Ultra-long Cycle Life Enabled by the ZnI_2 Additive. ACS Sustain. Chem. Eng. **9**, 13268–13276 (2021).
22. Wu, W. et al. Electrode and electrolyte regulation to promote coulombic efficiency and cycling stability of aqueous zinc-iodine batteries. Chem. Eng. J. **428** (2022).
23. Xu, J. et al. ZIF-8 derived porous carbon to mitigate shuttle effect for high performance aqueous zinc-iodine batteries. J. Colloid Interface Sci. **610**, 98–105 (1800).
24. Yan, L. et al. Multifunctional porous carbon strategy assisting high-performance aqueous zinc-iodine battery. Carbon **187**, 145–152 (2022).
25. Zhao, Y., Wang, L. & Byon, H.R. High-performance rechargeable lithium-iodine batteries using triiodide/iodide redox couples in an aqueous cathode. Nat. Commun. **4** (2013).
26. Wang, S. et al. Insight into MoS_2-MoN Heterostructure to Accelerate Polysulfide Conversion toward High-Energy-Density Lithium-Sulfur Batteries. Adv. Energy Mater. **11** (2021).
27. Bai, C. et al. A sustainable aqueous Zn-I_2 battery. Nano Res. **11**, 3548–3554 (2018).
28. Lu, K. et al. Sulfur and nitrogen enriched graphene foam scaffolds for aqueous rechargeable zinc-iodine battery. Electrochim. Acta **296**, 755–761 (2019).
29. Dai, C. et al. A Cascade Battery: Coupling Two Sequential Electrochemical Reactions in a Single Battery. Adv. Mater. **33** (2021).
30. Xu, J. et al. Potassium-based electrochemical energy storage devices: Development status and future prospect. Energy Stor. Mater. **34**, 85–106 (2021).
31. Han, C., Zhu, J., Zhi, C. & Li, H. The rise of aqueous rechargeable batteries with organic electrode materials. J. Mater. Chem. A **8**, 15479–15512 (2020).
32. Han, C., Li, H., Li, Y., Zhu, J. & Zhi, C. Proton-assisted calcium-ion storage in aromatic organic molecular crystal with coplanar stacked structure. Nat. Commun. **12** (2021).
33. Zhang, Z. et al. Rechargeable Mg-Ion Full Battery System with High Capacity and High Rate. ACS Appl. Mater. Interfaces **13**, 40451–40459 (2021).
34. Jiang, L. et al. Building aqueous K-ion batteries for energy storage. Nat. Energy **4**, 495–503 (2019).
35. Gao, H. & Goodenough, J.B. An Aqueous Symmetric Sodium-Ion Battery with NASICON-Structured $Na_3MnTi(PO_4)_{(3)}$. Angew. Chem. Int. Ed. **55**, 12768–12772 (2016).
36. Cao, L. et al. Fluorinated interphase enables reversible aqueous zinc battery chemistries. Nat. Nanotechnol. **16**, 902-+ (2021).
37. Elimelech, M. & Phillip, W.A. The Future of Seawater Desalination: Energy, Technology, and the Environment. Science **333**, 712–717 (2011).
38. Qiao, J. et al. Long-Life Aqueous H^+/K^+ Dual-Cation Batteries Based on Dipyridophenazine//Hexacyanoferrate Electrodes. ACS Appl. Energy Mater. **4**, 4903–4909 (2021).
39. Wang, M., Wang, H., Zhang, H. & Li, X. Aqueous K -ion battery incorporating environment -friendly organic compound and Berlin green. J. Energy Chem. **48**, 14–20 (2020).

40. Li, Y. et al. An ultra-long life aqueous full K-ion battery. J. Mater. Chem. A **9**, 2822–2829 (2021).
41. Lu, K., Zhang, H., Gao, S., Cheng, Y. & Ma, H. High rate and stable symmetric potassium ion batteries fabricated with flexible electrodes and solid-state electrolytes. Nanoscale **10**, 20754–20760 (2018).
42. Liang, G. et al. Reconstructing Vanadium Oxide with Anisotropic Pathways for a Durable and Fast Aqueous K-Ion Battery. ACS nano (2021).
43. Deng, W., Shen, Y., Qian, J., Cao, Y. & Yang, H. A Perylene Diimide Crystal with High Capacity and Stable Cyclability for Na-Ion Batteries. ACS Appl. Mater. Interfaces **7**, 21095–21099 (2015).
44. Bai, Y. et al. Perylenetetracarboxylic diimide as a high-rate anode for potassium-ion batteries. J. Mater. Chem. A **7**, 24454–24461 (2019).
45. Li, S. et al. Sandwich-Like Heterostructures of MoS_2/Graphene with Enlarged Interlayer Spacing and Enhanced Hydrophilicity as High-Performance Cathodes for Aqueous Zinc-Ion Batteries. Adv. Mater. **33** (2021).
46. Sun, B. et al. A Passionfruit-Like Carbon-Confined Cu_2ZnSnS_4 Anode for Ultralong-Life Sodium Storage. Adv. Energy Mater. **11** (2021).
47. Zeng, X. et al. Anchoring Polyiodide to Conductive Polymers as Cathode for HighPerformance Aqueous Zinc-Iodine Batteries. ACS Sustain. Chem. Eng. **8**, 14280–14285 (2020).
48. Zhu, Z., Meng, Y., Cui, Y. & Chen, W. An Ultrastable Aqueous Iodine-Hydrogen Gas Battery. Adv. Funct. Mater. **31** (2021).
49. Meng, Z. et al. Ultra-stable binder-free rechargeable Li/I_2 batteries enabled by "Betadine" chemical interaction. Chem. Commun. **54**, 12337–12340 (2018).
50. Wang, F. et al. Fully Conjugated Phthalocyanine Copper Metal-Organic Frameworks for Sodium-Iodine Batteries with Long-Time-Cycling Durability. Adv. Mater. **32** (2020).
51. Lu, K. et al. Rechargeable potassium-ion batteries enabled by potassium-iodine conversion chemistry. Energy Stor. Mater. **16**, 1–5 (2019).
52. Sun, C. et al. $Ti_3C_2T_x$ MXene Interface Layer Driving Ultra-Stable Lithium-Iodine Batteries with Both High Iodine Content and Mass Loading. ACS Nano **14**, 1176–1184 (2020).
53. Tian, H. et al. High power rechargeable magnesium/iodine battery chemistry. Nat. Commun. **8** (2017).
54. Tian, H., Zhang, S., Meng, Z., He, W. & Han, W.-Q. Rechargeable Aluminum/Iodine Battery Redox Chemistry in Ionic Liquid Electrolyte. ACS Energy Lett. **2**, 1170–1176 (2017).
55. Li, W., Wang, K. & Jiang, K. A high energy efficiency and long life aqueous Zn-I_2 battery. J. Mater. Chem. A **8**, 3785–3794 (2020).
56. Li, H., Li, M., Zhou, X. & Li, T. A novel rechargeable iodide ion battery with zinc and copper anodes. J. Power Sources **449** (2020).
57. Wessells, C.D., Peddada, S.V., Huggins, R.A. & Cui, Y. Nickel Hexacyanoferrate Nanoparticle Electrodes For Aqueous Sodium and Potassium Ion Batteries. Nano Lett. **11**, 5421–5425 (2011).

58. J. Shamir, R.R. Laser Raman spectrum of the dichloroiodinium($IC1_2^+$) cation. Spectrochimi. Acta A **29**, 873–878.
59. Wang, Y. et al. Binding Zinc Ions by Carboxyl Groups from Adjacent Molecules toward Long-Life Aqueous Zinc-Organic Batteries. Adv. Mater. **32** (2020).
60. Hao, J. et al. Boosting Zinc Electrode Reversibility in Aqueous Electrolytes by Using Low-Cost Antisolvents. Angew. Chem. Int. Ed. **60**, 7366–7375 (2021).
61. Zhang, C. et al. A $ZnCl_2$ water-in-salt electrolyte for a reversible Zn metal anode. Chem. Commun. **54**, 14097–14099 (2018).
62. Suo, L. et al. "Water-in-salt" electrolyte enables high-voltage aqueous lithium-ion chemistries. Science **350**, 938–943 (2015).
63. Yue, J. et al. Aqueous interphase formed by CO_2 brings electrolytes back to salt-in-water regime. Nat. Chem. **13**, 1061-+ (2021).
64. Lukatskaya, M.R. et al. Concentrated mixed cation acetate "water-in-salt" solutions as green and low-cost high voltage electrolytes for aqueous batteries. Energy Environ. Sci. **11**, 2876–2883 (2018).
65. Hou, X. et al. Simultaneous Formation of Interphases on both Positive and Negative Electrodes in High-Voltage Aqueous Lithium-Ion Batteries. Small (2021).
66. Nian, Q. et al. An Overcrowded Water-Ion Solvation Structure for a Robust Anode Interphase in Aqueous Lithium-Ion Batteries. ACS Appl. Mater. Interfaces **13**, 51048–51056 (2021).
67. Zhou, A. et al. TiO_2 (B) anode for high-voltage aqueous Li-ion batteries. Energy Stor. Mater. **42**, 438–444 (2021).
68. Shi, H.-Y. et al. Accessing the 2 V V^{V}/V^{IV} redox process of vanadyl phosphate cathode for aqueous batteries. J. Power Sources **507** (2021).
69. Hou, X. et al. Stabilizing the Solid-Electrolyte Interphase with Polyacrylamide for High-Voltage Aqueous Lithium-Ion Batteries. Angew. Chem. Int. Ed. **60**, 22812–22817 (2021).
70. Pan, W. et al. High-Energy SWCNT Cathode for Aqueous Al-Ion Battery Boosted by Multi-Ion Intercalation Chemistry. Adva. Energy Mater. **11** (2021).
71. Pan, W. et al. High-Performance MnO_2/Al Battery with In Situ Electrochemically Reformed Al_xMnO_2 Nanosphere Cathode. Small Methods **5** (2021).
72. Wang, X. et al. High-voltage aqueous planar symmetric sodium ion micro-batteries with superior performance at low-temperature. Nano Energy **82** (2021).
73. Li, Y. et al. A Superconcentrated Water-in-Salt Hydrogel Electrolyte for High-Voltage Aqueous Potassium-Ion Batteries. Chemelectrochem **8**, 1451–1454 (2021).
74. Hou, X. et al. TiO_2@$LiTi_2(PO_4)_{(3)}$ enabling fast and stable lithium storage for high voltage aqueous lithium-ion batteries. J. Power Sources **484** (2021).
75. Li, T., Li, M., Li, H. & Zhao, H. High-voltage and long-lasting aqueous chlorine-ion battery by virtue of "water-in-salt" electrolyte. Iscience **24** (2021).

76. Reber, D., Grissa, R., Becker, M., Kuhnel, R.-S. & Battaglia, C. Anion Selection Criteria for Water-in-Salt Electrolytes. Adva. Energy Mater. **11** (2021).
77. Zhao, J. et al. High-voltage Zn/$LiMn_{0.8}Fe_{0.2}PO_4$ aqueous rechargeable battery by virtue of "water-in-salt" electrolyte. Electrochem. Commun. **69**, 6–10 (2016).
78. Hu, P. et al. Zn/V_2O_5 Aqueous Hybrid-Ion Battery with High Voltage Platform and Long Cycle Life. ACS Appl. Mater. Interfaces **9**, 42717–42722 (2017).
79. Yang, C. et al. Flexible Aqueous Li-Ion Battery with High Energy and Power Densities. Adv. Mater. **29** (2017).
80. Xie, J., Liang, Z. & Lu, Y.-C. Molecular crowding electrolytes for high-voltage aqueous batteries. Nat. Mater. **19**, 1006-+ (2020).
81. Adamo, C., Scuseria, G.E. & Barone, V. Accurate excitation energies from time-dependent density functional theory: Assessing the PBE0 model. J. Chem. Phys. **111**, 2889–2899 (1999).
82. Frish, M. et al. Gaussian 09, revision A. 02. Gaussian Inc., Wallingford CT (2009).
83. Zhu, J. & Ji, P. Dispersion relation and Landau damping of waves in high-energy density plasmas. Plasma Phys. Controlled Fusion **54** (2012).
84. Marenich, A.V., Cramer, C.J. & Truhlar, D.G. Universal Solvation Model Based on Solute Electron Density and on a Continuum Model of the Solvent Defined by the Bulk Dielectric Constant and Atomic Surface Tensions. J. Phys. Chem. B **113**, 6378–6396 (2009).

Figures

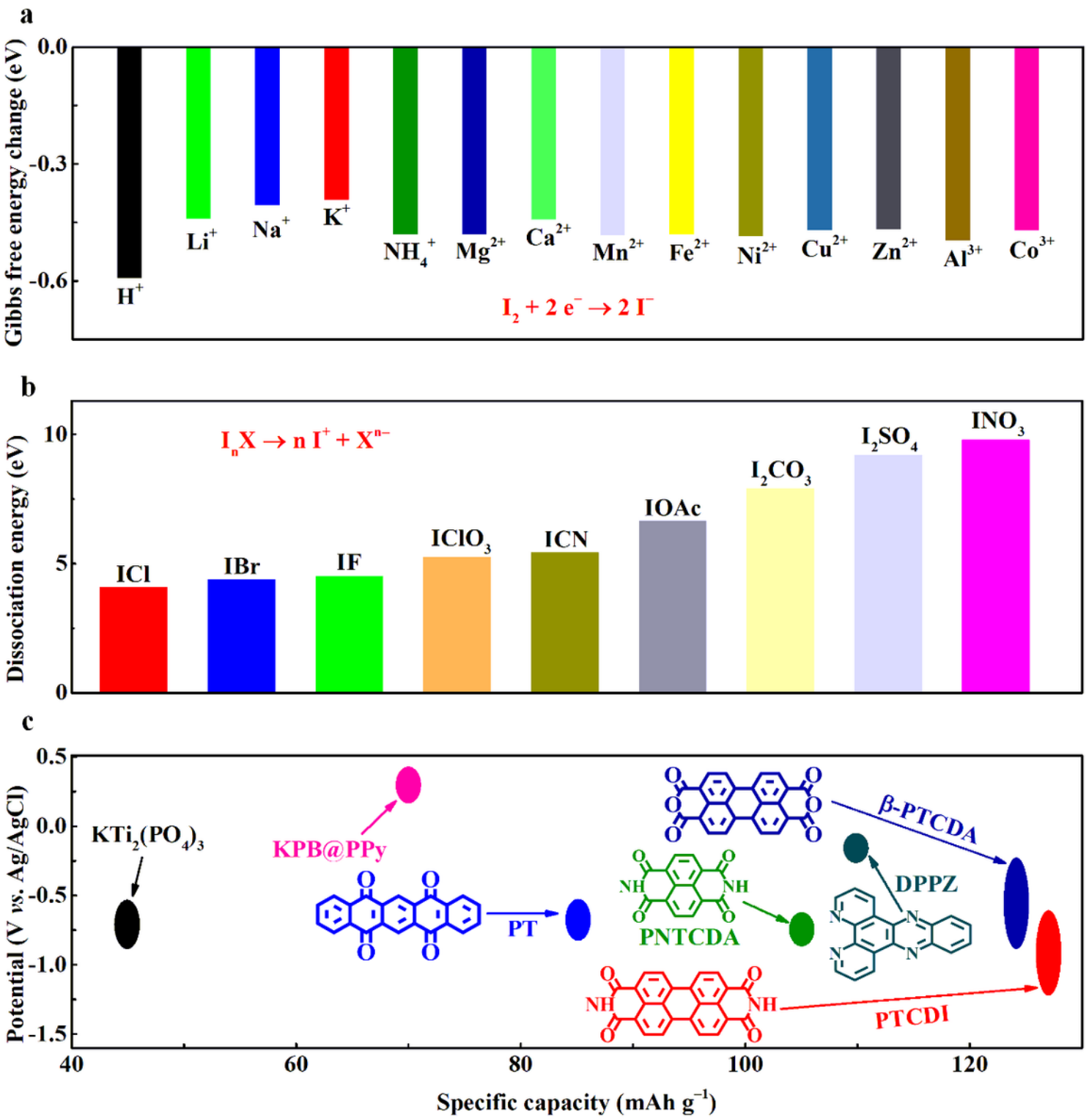

Figure 1

a, Comparison of the calculated Gibbs free energy change of I^-/I^0 conversion in different cations environment. **b,** Comparison of the calculated dissociation energy of various iodine compounds. **c,** The charge/discharge potential range and specific capacity of anodes with K^+ insertion/de-insertion chemistry.

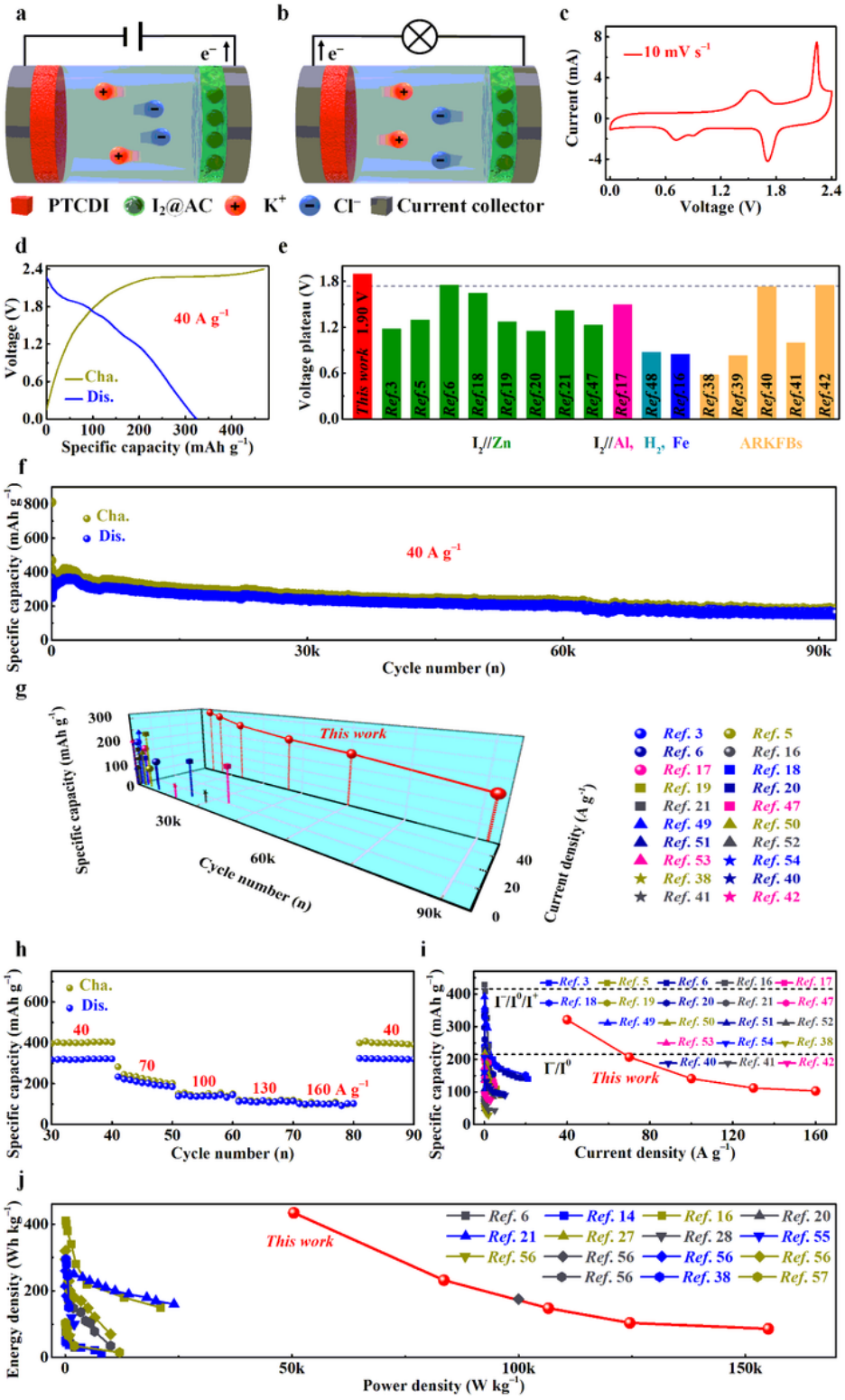

Figure 2

a–b, Schematics of reaction mechanism of the PTCDI//I_2 full cell in saturated KCl electrolyte during charging and discharging processes, respectively. **c–d,** The typical CV and GCD profiles of the full cell, respectively. The specific capacity was calculated based on the mass loading of I_2 in I_2@AC cathode. **e,** Comparison of the discharge voltage plateau among reported works. **f,** Cycling performance of the full

cell at 40 A g^{-1}. **g,** Cycling performance comparison with literatures on aqueous I_2-cathode based batteries and ARKFBs. **h,** The rate capability at different current densities. **i,** Rate capability comparison with literatures on aqueous I_2-cathode based batteries and ARKFBs. **j,** Ragone plots of this work compared to the previously reported aqueous I_2-cathode based batteries and ARKFBs.

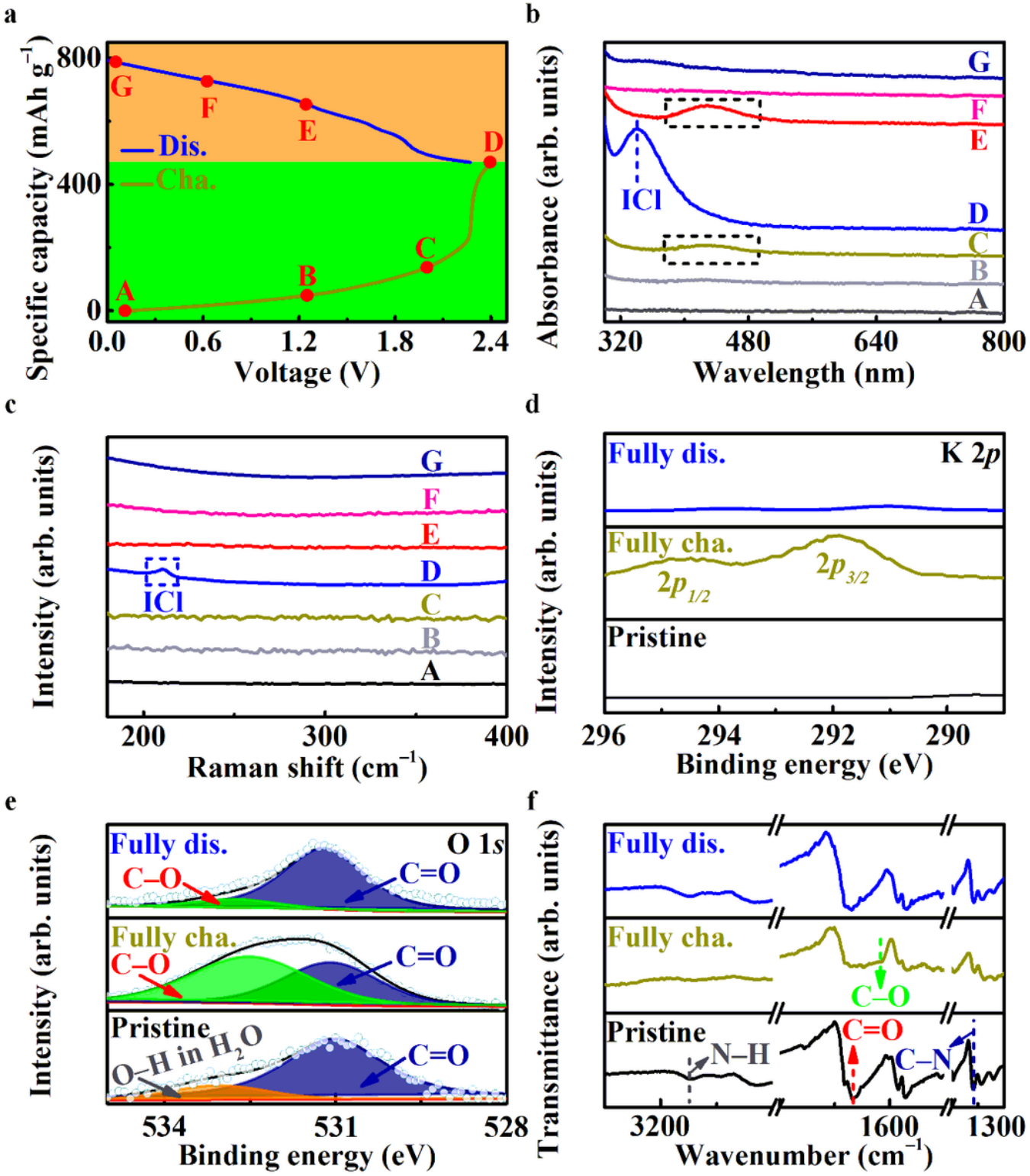

Figure 3

a, GCD curve of the PTCDI//I_2 full cell with marked voltage points for characterizations. **b,** UV-*vis* spectra of the utilized electrolyte recorded at varied charge/discharge stages. **c,** Raman spectra of the I_2 electrode recorded at different charge/discharge states. **d–f,** High-resolution K 2*p* XPS spectra, O 1*s* XPS spectra, and FT-IR spectra of the PTCDI anode at pristine, fully charged and fully discharged states, respectively.

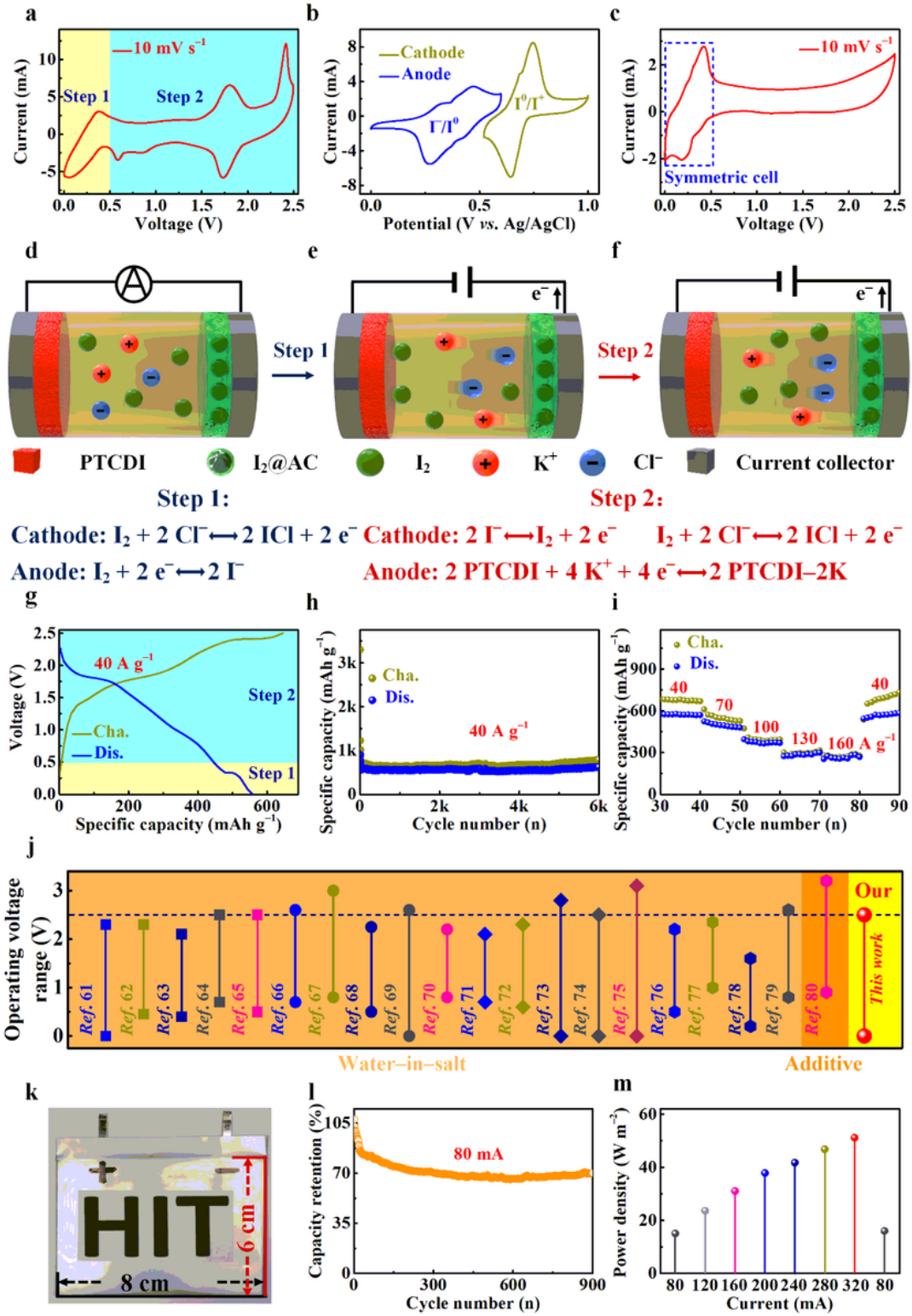

Figure 4

a, The typical CV curve of the PTCDI//I_2 cascade cell in saturated KCl+I_2(aq) mixed electrolyte. **b,** The typical CV curves of the graphite paper (GP) substrate in a three-electrode system (working electrode: GP; counter electrode: platinum; reference electrode: standard Ag/AgCl electrode). **c,** The typical CV curve of the GP//GP symmetric battery in saturated KCl+I_2(aq) mixed electrolyte. **d–f,** Schematic illustration of the PTCDI//I_2 cascade cell in saturated KCl+I_2(aq) electrolyte at pristine, the first charge step and the second charge step, respectively. **g–i,** The typical GCD curve, cycling performance and rate capability of the PTCDI//I_2 cascade cell in saturated KCl+I_2(aq) mixed electrolyte, respectively. The specific capacity was calculated based on the mass loading of I_2 in I_2@AC cathode. **j,** Comparison of the operating voltage range between this work and literatures on high-voltage aqueous batteries. **k–m,** Photograph, capacity retention, and rate capability of the PTCDI//GP cathode-free cascade cell in saturated KCl+I_2(aq) mixed electrolyte, respectively.

Supplementary Files

This is a list of supplementary files associated with this preprint. Click to download.

- SupportingInformation.docx